

Characterization and *In Vitro* Corrosion Investigations of Thermal Sprayed Hydroxyapatite and Hydroxyapatite-Titania Coatings on Ti Alloy

TEJINDER PAL SINGH SARAO, HAZOOR SINGH SIDHU, and HARPREET SINGH

In the current investigation, hydroxyapatite (HA) powder was mixed with titania (TiO₂) in 50:50 wt pct for depositing composite coatings on a Ti-alloy substrate using a thermal-spray coating technique. The coatings were characterized by X-ray diffraction (XRD) and scanning electron microscopy (SEM)/energy-dispersive X-ray spectroscopy (EDS) analyses. The corrosion behavior of the coatings was studied by electrochemical corrosion testing in simulated human body fluid. After the corrosion testing, the samples were analyzed by XRD and SEM/EDS analyses. HA and TiO₂ (rutile) were the main phases observed in the developed coatings. Bulk HA coating was amorphous; however, the addition of TiO₂ effectively improved the crystallinity of HA in HA-TiO₂ coating. The SEM analysis confirmed the formation of a well-formed HA-TiO₂ composite coating. HA coating exhibited higher bond strength (67.8 MPa) compared with HA-TiO₂ composite coating (37.6 MPa). The electrochemical study showed a significant improvement in the corrosion resistance of the Ti alloy after the deposition of the coatings.

DOI: 10.1007/s11661-012-1175-8

© The Minerals, Metals & Materials Society and ASM International 2012

I. INTRODUCTION

METALS with excellent mechanical properties and reasonable biocompatibility are widely used as biomedical implants. The ultimate goal of using biomaterials in medicine is to restore the function of natural living tissues and organs in the human body.^[1] Pure titanium (Ti) and its alloy Ti-6Al-4V (wt pct) [Ti-6-4] are the most widely used materials for biomedical applications because of their good fatigue strength, excellent biocompatibility, and corrosion resistance.^[2] Besides the formation of a highly stable TiO₂ layer in Ti-6-4, the oxides of Al and V form an additional passive layer, causing subsequent resistance against corrosion.^[3] The stability of the surface oxide layer is one of the most important features of a biomaterial.^[4] The composition of the surface oxide layer changes because of reactions between the implant surface and living tissues.^[5] The two major issues regarding the long-term use of metallic implants in highly aggressive human body environment are corrosion of metallic implants and the lack of integration of metallic implants with human tissues.^[6]

Surface coating or modification is one alternative that has been widely considered for improving the mechanical, chemical, and biological properties of Ti and its alloys for biomedical applications.^[7] The coating of biomaterials with calcium phosphate (CaP)-based hydroxyapatite (HA) (Ca₁₀(PO₄)₆(OH)₂) has attracted wide interest from both the orthopedic and dental fields in clinical applications because of its excellent biocompatibility and tissue bioactivity properties.^[8] Osteoconductive CaP coatings promote bone healing leading to the rapid biological fixation of implants.^[9]

Currently, the plasma spraying process is used for depositing HA on bioimplants. Although it improves the bone strength and initial osseointegration, still optimum coating properties with maximum bone response are yet to be achieved.^[10] It has been reported that elevated temperatures in plasma spraying result in the alteration of structural properties, peeling, and subsequent dis-solution of the coating, which further reduce the bond strength between the coating and substrate. Moreover, because of the number of process parameters,^[10,11] intensive work is being conducted to overcome the problems of existing plasma spray process and to create more stable HA coatings by alternative coating techniques. This study is a step towards this direction, in which a proprietary thermal-spray equipment has been used to deposit the coatings on the Ti alloy.

An alternative approach for improving the mechanical, chemical and biological properties of Ti and its alloys, is the use of bond or composite coatings. Titania (TiO₂), zirconia (ZrO₂), and alumina (Al₂O₃) are used as bond coats or as composite coats with HA in different ratios to enhance the mechanical and biological

TEJINDER PAL SINGH SARAO, Associate Professor, is with the Department of Mechanical Engineering, Gulzar Institute of Engineering & Technology, Khanna, Punjab 141402, India. HAZOOR SINGH SIDHU, Associate Professor, is with the Department of Mechanical Engineering, Yadavindra College of Engineering, Punjabi University, Talwandi sabo, Punjab 151302, India. HARPREET SINGH, Assistant Professor, is with the School of Mechanical, Materials, and Energy Engineering, Indian Institute of Technology Ropar, Rupnagar, Punjab 140001, India. Contact e-mails: harpreetsingh@iitrpr.ac.in; hnr97@yahoo.com

Manuscript submitted August 25, 2011.

Article published online May 22, 2012

properties of HA coatings.^[12–14] TiO₂ has attracted much attention as a composite or bond coat material because of its biological and corrosion-resistance effects.^[15] The melting point of TiO₂ [2116 K (1843 °C)] is much lower than that of Al₂O₃ and ZrO₂, which are above 2273 K (2000 °C). The relatively lower melting point of TiO₂ is helpful in the formation of a homogeneous HA-TiO₂ composite coating. Moreover, HA has lower thermal diffusivity (α) and conductivity (k) values than those of TiO₂. Therefore, TiO₂ particles need lower thermal energy to reach a given temperature compared with that of HA. To improve the thermal mismatch between HA coating and Ti substrate, the addition of TiO₂ is favorable.^[16]

Several earlier studies^[17–23] have reported an increase in the mechanical and biological properties of the HA-TiO₂ composite coatings than the HA coatings. In high-velocity oxygen fuel (HVOF) sprayed HA-TiO₂ composite coatings, the addition of TiO₂ is found to improve the Young's modulus, fracture toughness, and shear strength of HVOF-sprayed HA-based coatings. It was suggested that addition of less than 20 vol pct TiO₂ is suitable for satisfactory toughening of HA coatings.^[12,24] Ramires *et al.*^[18] reported that the sol-gel fabricated HA-TiO₂ coatings were not cytotoxic and allowed the proliferation of human osteoblast like cells. Kim *et al.*^[25] suggested that the sol-gel deposited HA-TiO₂ composite coatings possess excellent properties for hard tissue applications from the mechanical and biological perspective.

In the current work, a proprietary flame-spray system has been used to deposit HA and HA-TiO₂ coatings on a Ti alloy. Subsequently, the corrosion behavior of uncoated, HA-coated, and HA-TiO₂-coated alloy has been investigated. The corrosion tests were conducted by an electrochemical potentiodynamic method in a simulated body fluid (Ringer's solution).

II. EXPERIMENTAL DETAILS

A. Deposition of Coatings

A commercially available biomedical material titanium-aluminum-vanadium alloy (Ti-6-4, ASTM F-136) having chemical composition in wt pct — N: 0.02; C: 0.05; H: 0.01; Fe: 0.20; O: 0.16, Al: 6.10; V: 3.95 and Ti: balance, was used as the substrate material in this study. Disc shaped Ti-6-4 specimens each measuring 12 mm × 5 mm were prepared for the studies. The specimens were polished by silicon carbide papers down to 180 grit followed by cloth wheel polishing with alumina paste on a polishing machine. These specimens were washed with deionized water followed by acetone rinsing. The substrates were then grit blasted using grit blasting equipment (Pressure Blaster 9182; Surface International, Jodhpur, India). Al₂O₃ grits of 20 mesh size were used during the grit-blasting operation at a pressure of 5 bars for 2 minutes. The substrates were subsequently air blasted to remove any residual grit. The HA powder (Captal S; Plasma Biotol, Derbyshire, U.K.) of 10 μm average particle size and TiO₂ powder (Amperit 782.0;

H.C. Starck GmbH, Goslar, Germany) with a particle size distribution from 5 to 22 μm were used in this study. Both the powders (HA and TiO₂) were mixed mechanically in the ratio of 50:50 (wt pct). The Ti-6-4 specimens were thermal sprayed using flame-spray system (CERAJET) at Metalizing Equipment Company Private Limited (MECPL; Jodhpur, India). CERAJET is proprietary product of MECPL, specially designed for ceramic coatings. The particle velocity of conventional flame-spraying systems is less than 100 m/s, whereas the particle velocity of the current flame-spray system is ≈300 m/s. The temperature of oxyacetylene flames in CERAJET system is ≈2973 K (2700 °C), which is much lower than the plasma spraying technique. The spraying parameters used for both HA and HA-TiO₂ coatings are given in Table I.

The thermal spraying of composite powder was carried out immediately after grit blasting of substrates. The coating thickness to be achieved was targeted in a range of 150 to 200 μm.

B. Characterization of the Coatings

The phase composition of the starting powder as well as the as-sprayed coatings was analyzed using an X'pert-PRO (PANalytical B.V., Almelo, the Netherlands) X-ray diffractometer (XRD) with Cu K_α radiation, operating at 40 KV/30 mA. The coated samples were scanned over 2θ range of 20 deg to 60 deg. The morphology of feedstock powders and as-sprayed specimens was examined by using QUANTA 200 field-emission gun (FEI Corporation, Hillsboro, OR, scanning electron microscope (SEM) coupled with an energy-dispersive spectroscope (EDS). After surface characterization, the samples were sectioned with a low-speed precision saw at 75 rpm speed and mounted in an epoxy resin using a specimen mounting press. The mounted samples were polished with emery papers of 220, 400, 600, and 800 grade and subsequently 1/0, 2/0, 3/0, and 4/0 grades. Then samples were mirror polished with slurry of alumina on a napped cloth to highlight the surface of the coated substrates. The samples were gold plated to achieve the desired conductivity before observation in SEM. A surface as well as a cross-sectional SEM/EDS analysis of the coated samples was done to study their elemental compositions along with the microstructural features. EDS elemental maps were obtained to display the distribution of elements in the coating on JEOL JSM-6610LV SEM (JEOL Ltd., attached with OXFORD Instruments EDS (Oxfordshire, U.K.).

Table I. Thermal Spray Process Parameters for HA and HA-TiO₂ Coatings

Spraying Parameter	Value
Acetylene flow rate (l min ⁻¹)	73
Oxygen flow rate (l min ⁻¹)	44
Air pressure (kg cm ⁻²)	4.5
Powder feed rate (g min ⁻¹)	15
Spray distance (cm)	10

C. Surface Roughness

The surface roughness of Al_2O_3 blasted, HA-coated, and HA- TiO_2 coated Ti-6-4 samples was measured by a roughness tester (SJ-400; MITUTOYO America Corporation, Aurora, IL), using a filter of Gaussian type and roughness standard JIS1994 for a cut-off length (λc) of 0.8 mm. Each reported value of roughness is the average of five measurements at various positions on the surface of the coated samples. The measured roughness parameters are Ra (the arithmetic mean of departures of the roughness profile from the mean line), Rq (root mean square [RMS] of average roughness), and Rz (average of the highest peaks and the lowest valleys on five measurement lengths). Among these parameters, Ra is the most commonly used roughness parameter.

D. Bond Strength

The bond strength of both the coatings on stainless steel (SS) specimens is determined as per ASTM-C633 standard for thermal-spray coatings. For this test, identical cylindrical SS rod (25.4 mm diameter) specimens were prepared. HA coatings of thickness $\approx 300 \mu\text{m}$ and HA- TiO_2 coating of thickness $\approx 350 \mu\text{m}$ were deposited on SS rods by the flame-spray system (CERAJET). The flat surface of the uncoated rod was grit blasted and bonded to the coated rod by a special adhesive glue. The assembly was given a heat treatment to cure and harden the bonding glue and tested on a universal testing machine. Each reported value of bond strength is the average of three measurements.

E. Electrochemical Measurements

Electrochemical techniques are preferred to measure the corrosion rate of implant materials as these techniques are quick and sensitive to measure even a low corrosion rate. To investigate the electrochemical corrosion behavior of the uncoated, HA-coated, and HA- TiO_2 -coated Ti-6-4 specimens, a potentiodynamic polarization test was conducted using a Potentiostat/Galvanostat (Series G-750; Gamry Instruments, Warminster, PA), interfaced to a computer and supported with Gamry electrochemical software DC105. The electrolyte used for simulating human body fluid conditions was Ringer's solution with chemical composition (in g/L) as 9-NaCl, 0.24- CaCl_2 , 0.43-KCl, and 0.2- NaHCO_3 at pH 7.2. Before conducting the corrosion studies, each specimen was immersed in Ringer's solution for 24 hours for stabilization. In the electrochemical cell, each specimen was kept such that it remained just below the surface of Ringer's solution for *in vitro* potentiodynamic corrosion tests. All the experiments were conducted in Ringer's solution at a temperature of $310 \text{ K} \pm 1 \text{ K}$ ($37 \text{ }^\circ\text{C} \pm 1 \text{ }^\circ\text{C}$), which is the normal temperature of human body. The temperature was maintained using a heating mantle. The exposed area of the samples in the Ringer's solution was 1 cm^2 . The Ti-6-4 specimen formed the working electrode. All potentials were measured with respect to a saturated calomel electrode (SCE) as the reference

electrode. A graphite rod served as the counterelectrode. All tests were performed at a scan rate of 1 mV/sec and fresh solution was used for each experiment. Polarization curves were initiated at -250 mV below the open circuit potential and the tests were started after a steady open-circuit potential was achieved (not more than $\pm 5 \text{ mV}$ drift in 5 minutes). The corrosion rate was determined using the Tafel extrapolation method and all the tests were carried out on three fresh samples to verify repeatability of test results. In Tafel methods, tangents were drawn on graphical plot of E vs $\log I$, which on extrapolation to corrosion potential (E_{Corr}) intersected at a point, which on X axis gives the corrosion current (I_{Corr}) value. After corrosion testing, the specimens were analyzed by SEM/EDS and XRD techniques to analyze the microstructure/composition and phase formation, respectively.

III. RESULTS AND DISCUSSION

A. XRD Analysis

The XRD scans of HA and TiO_2 powders are shown in Figure 1. The scans indicate that both the HA and TiO_2 powders consist of crystalline phases in accordance

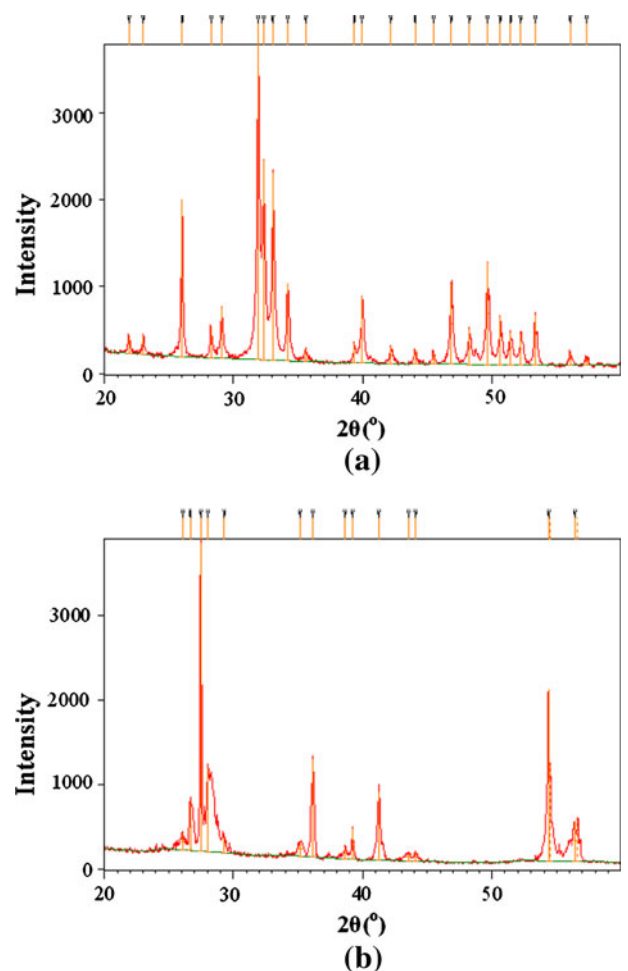
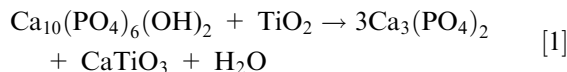


Fig. 1—X-ray diffraction pattern of (a) HA powder and (b) TiO_2 powder.

with JCPDS cards 9-432 and 21-1276, respectively. The analysis shows that all the major peaks belong to HA in Figure 1(a) and TiO₂ rutile phase in Figure 1(b). TiO₂ crystallizes in three major structures: rutile (tetragonal), anatase (tetragonal), and brookite (rhombohedral).^[15] The XRD analysis of the HA-TiO₂ composite powder is shown in Figure 2.

The XRD analysis for the flame-sprayed HA coating on Ti-6-4 substrate is shown in Figure 3(a). It is found that the XRD pattern of HA coatings is extremely different from that of the feedstock HA powder. A large hump is observed around 30 deg (2θ) showing amorphous structure without the appearance of any crystalline peak. The formation of the amorphous phase may be attributed to the fine particle size of HA powder, which might have melted completely during the thermal spraying. Previous literature reports that amorphous phases are more soluble than crystalline HA, which leads to rapid disintegration of HA coating from implant surface.^[26,27]

Interestingly, in HA-TiO₂ composite coatings as shown in Figure 3(b), the addition of TiO₂ effectively improved the crystallinity of HA in HA-TiO₂ coating; otherwise, the HA coating was amorphous. In HA-TiO₂ composite coatings, the coating structure mainly comprises HA and TiO₂ (rutile) phases. Besides the crystalline HA and TiO₂ phases, the as-sprayed coating consists of minor β-tri-calcium phosphate (β-TCP) phase, but no chemical products such as CaTiO₃ were detected from the XRD scans. The formation of CaTiO₃ is suggested to reduce adhesive strength and destroy the HA structure.^[12] In HVOF-sprayed HA-TiO₂ (anatase) composite coatings, the following chemical reaction at ~1683 K (1410 °C) temperature indicates the formation of CaTiO₃.^[12]



Of three polymorphic forms of titania, rutile is the only stable phase, whereas anatase and brookite are metastable and are transformed to rutile irreversibly by

heating.^[4] A previous study found that HA prefers to react chemically with anatase than rutile TiO₂.^[28]

B. SEM/EDS Analysis

1. Surface analysis

The morphology of the individual and composite feedstock powders is shown in Figure 4. The SEM micrographs show that HA powder particles are spherical, whereas TiO₂ powder particles are of angular and irregular shape. The size distribution range seems to be wider in both powders. It is worthwhile to mention that the particle shape, size, and morphology influence the final microstructure of the thermal-sprayed coatings.

The SEM micrograph along with EDS point analysis of an HA-coated specimen is shown in Figure 5. The microstructure in general consists of well-formed interconnected splats with uneven surface. There is a significant presence of unmelted particles, which have retained their spherical morphology. Some voids/pores can also be observed but no microcracks were observed on the coating surface. The EDS analysis as shown

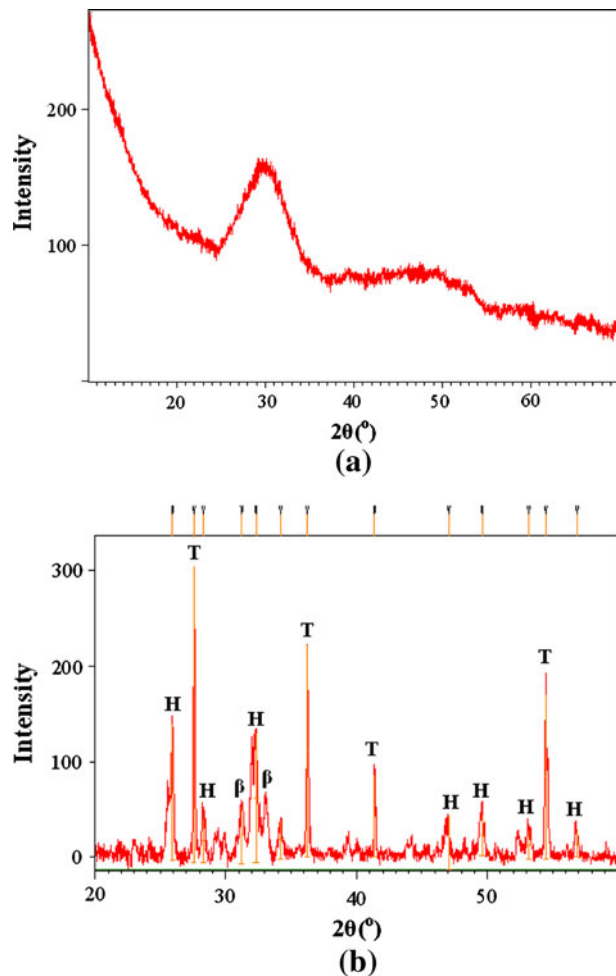


Fig. 3—X-ray diffraction pattern of flame-sprayed (a) HA coating and (b) HA-TiO₂ coating on Ti-6-4, [HA (H), TiO₂ rutile (T) and β-TCP (β)].

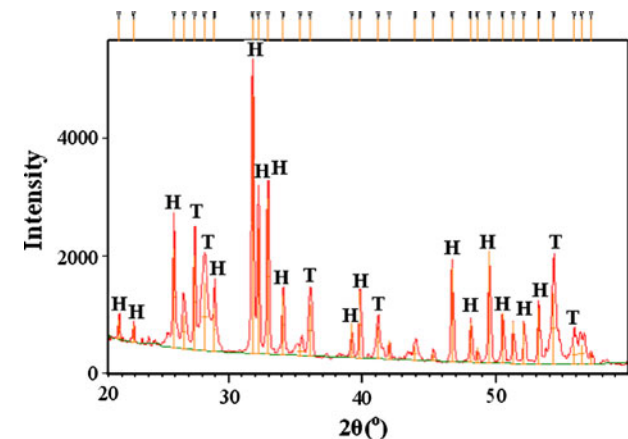


Fig. 2—X-ray diffraction pattern of HA-TiO₂ composite powder, [HA (H) and TiO₂ rutile (T)].

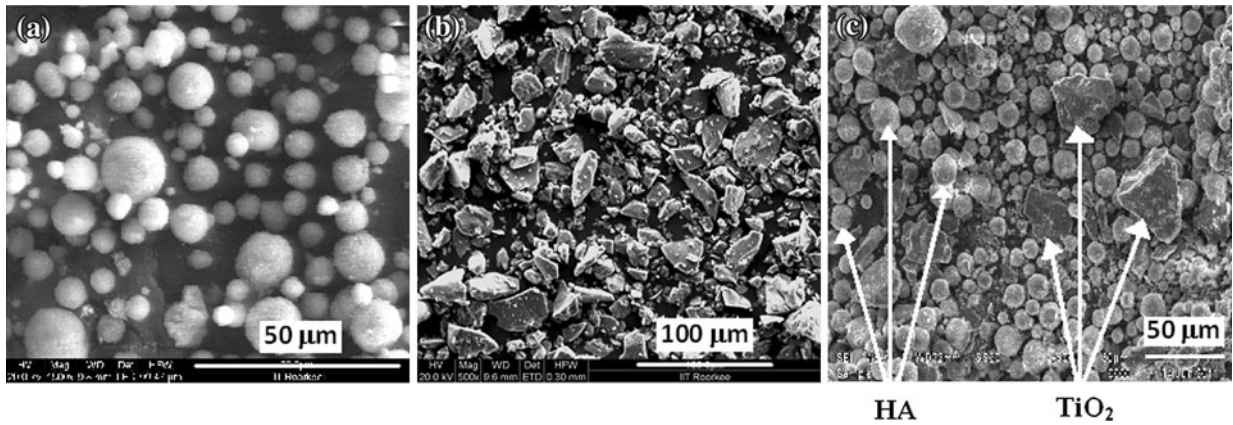


Fig. 4—SEM morphologies of (a) HA, (b) TiO₂, and (c) HA-TiO₂ composite powder.

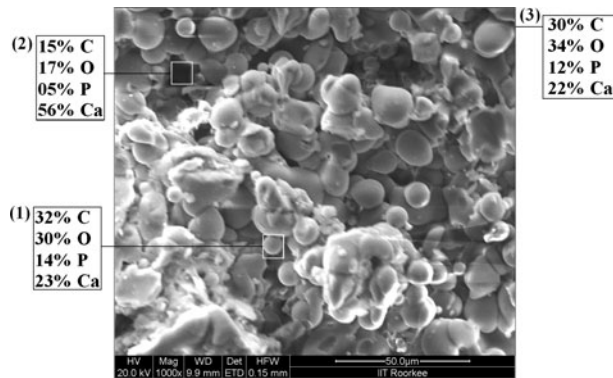


Fig. 5—Finite-element (FE)-SEM analysis along with EDS point analysis showing elemental composition of flame-sprayed HA coating on Ti-6-4.

in Figure 5 confirms the presence of calcium (Ca), phosphorous (P), carbon (C), and oxygen (O) elements with their atomic pct. The Ca/P ratio of feedstock HA powder is 1.67, which may change after thermal spraying. The Ca/P ratio of 1.64 (at point 1 in Figure 5) is characteristic for hydroxyapatite, which is close to the Ca/P ratio of 1.67. The observed different Ca/P ratios confirm the presence of phases other than HA in the as-sprayed coatings.

The HA-TiO₂ composite coating (Figure 6) consists of both nonmelted and semimelted powder particles. The coating microstructure seems to be uneven and heterogeneous. There is significant presence of some spherical particles, which may be of HA powder. The micrograph indicates that both the HA and TiO₂ powders have melted enough to form a dense composite coating. The difference in thermal conductivity of the TiO₂ (7.4 W/mK) and HA (1.25 W/mK) bulk materials shows that TiO₂ is a better heat conductor.^[29] Therefore, an HA particle needs more thermal energy to reach a given temperature level than needed for a TiO₂ particle.^[4] No microcrack was observed at the surface of the as-sprayed samples. The TiO₂ in the coating may have assisted in matching the thermal properties between the Ti-6-4 substrate and HA-TiO₂ composite coating. It seems that TiO₂ with a higher melting point ~2123 K (1850 °C) than

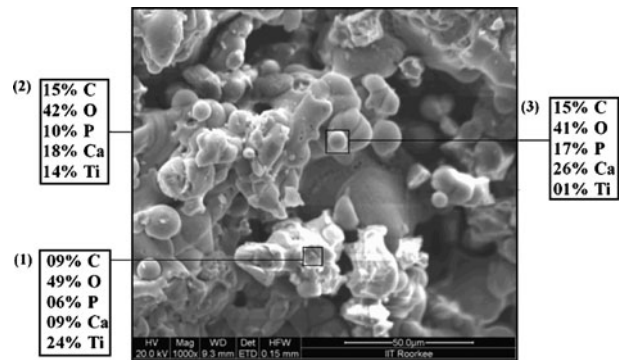


Fig. 6—FE-SEM analysis along with EDS point analysis showing elemental composition of flame-sprayed HA-TiO₂ coating on Ti-6-4.

that of HA ~1823 K (1550 °C) is melted enough to form a HA-TiO₂ composite coating.

EDS point analysis of HA-TiO₂ coating at different points indicates the presence of Ca, P, O, Ti, and C elements with their relative atomic pct values. The Ca/P ratio of 1.5 (at points 1 and 3 in Figure 6) indicates the formation of α -TCP and β -TCP. A point analysis of HA-TiO₂ coatings confirms that the spherical particles consist of HA. Both HA and TiO₂ seem to be well distributed throughout the HA-TiO₂ coating microstructure. A point analysis shows that Ca, P, and Ti elements coexist in different proportions in some melted particles.

2. Cross-sectional analysis

The cross-sectional EDS elemental map of flame-sprayed HA coating on the Ti-6-4 substrate is shown in Figure 7. Although because of the brittle nature of HA coatings there is a possibility of some HA coating particles getting removed during grinding and polishing process, these maps provide significant information about the distribution of various elements in the coatings. The mappings of Ca and P elements clearly demonstrated that these elements are distributed uniformly in the coating and are found to coexist in the coating region. O is present throughout the coating. The maps indicate that no diffusion of Ti and V elements from the substrate to the coating occurs; however, Al is present in the coating region

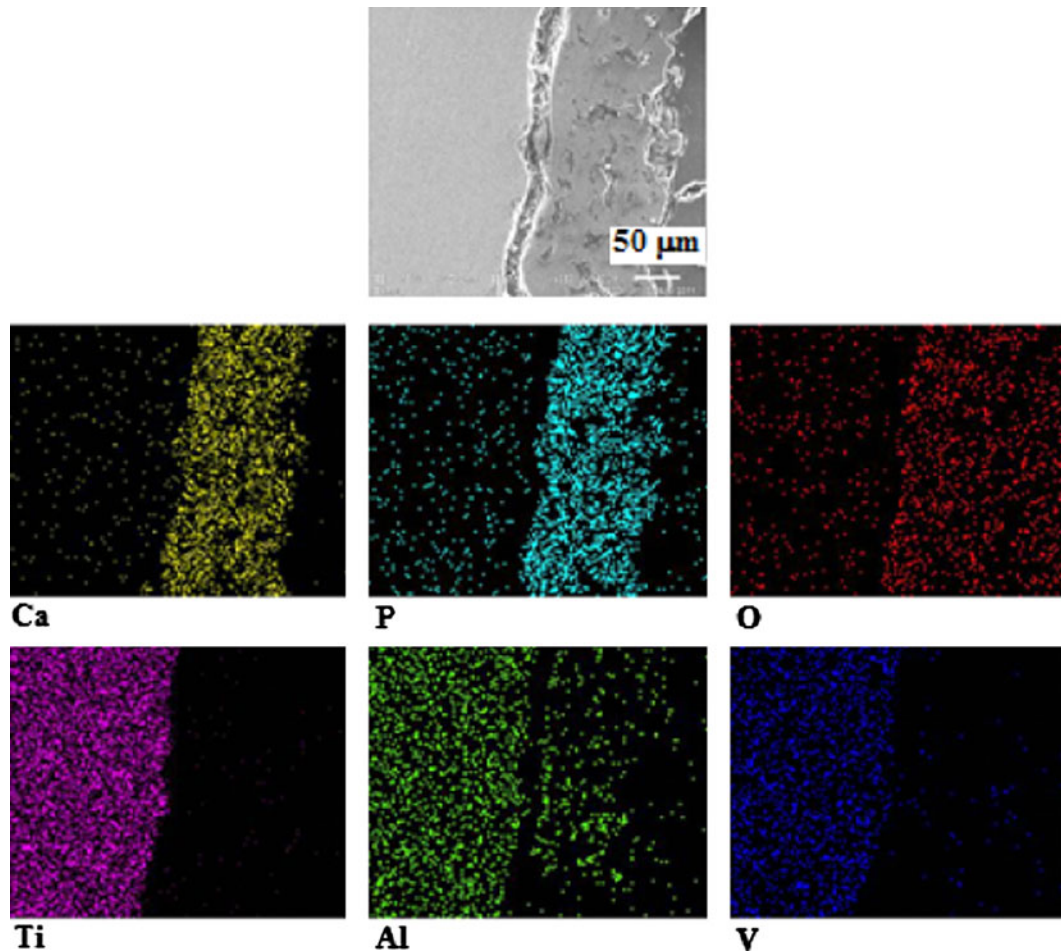


Fig. 7—Cross-sectional EDS elemental maps of flame-sprayed HA coating on Ti-6-4.

in a scattered manner. This may be because of the diffusion of Al from the substrate or artifacts of alumina polishing. The latter looks to be the more probable reason, as surface EDS measurements have not indicated the presence of Al, Ti, and V (Figure 5). The average value of the HA coating thickness measured from a cross-sectional micrograph is $120\ \mu\text{m}$. To understand the formation of cross-sectional microstructures in the composite coatings, EDS elemental maps (Figure 8) were used to differentiate between the HA and TiO_2 in the HA- TiO_2 coating. The average coating thickness measured from the SEM micrograph is found to be $140\ \mu\text{m}$. The coating contains mainly Ca, P, and Ti elements. The presence of Ti in both the coating as well as the substrate is obvious. Ca and P elements are found to coexist in the coating region. Wherever these elements are present, Ti is found to be absent and *vice versa*. These maps indicate that TiO_2 is dispersed as a particulate phase in the HA matrix, which means that a composite-like microstructure exists. Small diffusion of Al and V is also evident into the coating region.

C. Surface Roughness

Surface topography plays a significant role in the improvement of coating adhesion.^[30] Rough-surfaced implants favor both bone anchoring and biomechanical

stability.^[9] The surface roughness parameters (Ra, Rq, and Rz) for alumina-blasted, HA-coated, and HA- TiO_2 -coated substrates Ti-6-4 are shown in Figure 9. The average Ra value for blasted Ti-6-4 substrates was $4.00\ \mu\text{m}$, whereas in HA-coated Ti-6-4 it was $3.87\ \mu\text{m}$. In other words, the roughness values (Ra) of bare and HA-coated substrates do not differ significantly. Ra for HA- TiO_2 coated substrates was $8.04\ \mu\text{m}$, which is greater than roughness of HA-coated Ti-6-4 (Ra = $3.87\ \mu\text{m}$). The increase in roughness can be attributed to the presence of TiO_2 in the composite coating.

D. Bond Strength

The average bond strength of the current flame-sprayed HA coating was measured 67.8 MPa, which is much greater than the bond strength reported for other thermal-spray HA-coating techniques, as reported in Table II.

It is obvious that the technique used in the study could give relatively higher bond strengths compared with the reported techniques. The bond strength of the flame-sprayed HA- TiO_2 coating was found to be 37.6 MPa. The addition of 50 wt pct TiO_2 in the HA has drastically reduced the bond strength of the pure

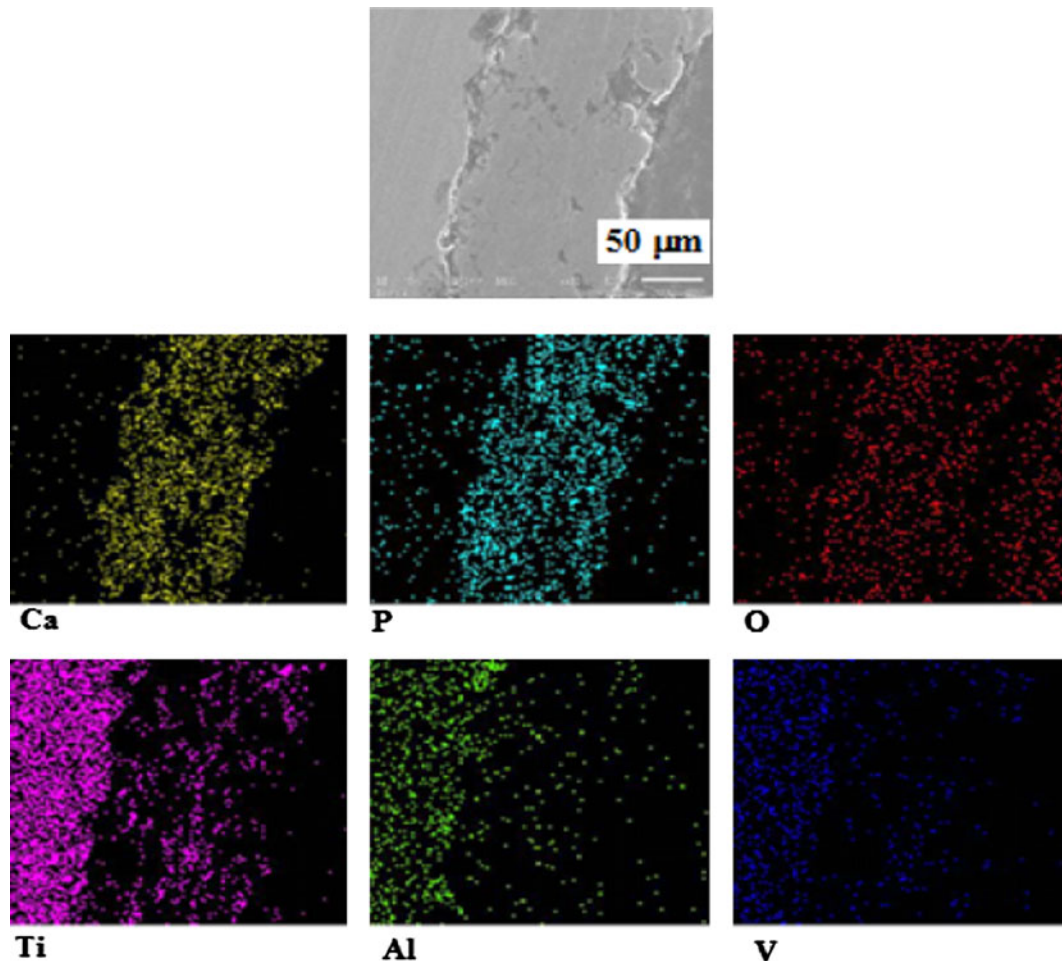


Fig. 8—Cross-sectional EDS elemental maps of flame-sprayed HA-TiO₂ coating on Ti-6-4.

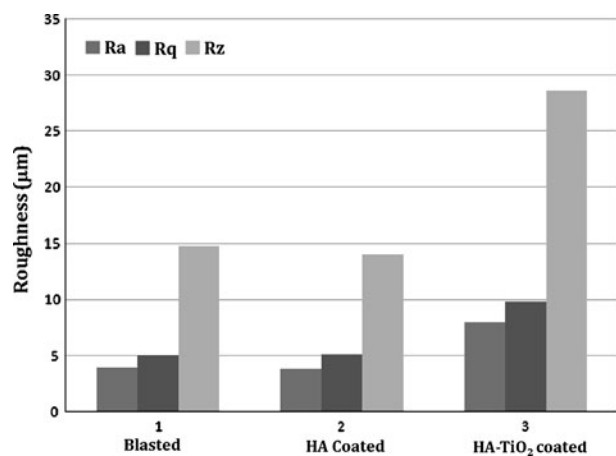


Fig. 9—Surface roughness measurements.

HA coating from 67.8 MPa to 37.6 MPa for HA-TiO₂ composite coating. Similar observations have been reported by Li *et al.*^[12] for HVOF-sprayed HA coatings on the Ti-6-4 substrate. They found that with the addition of 10 pct vol TiO₂, the adhesive strength decreased from 27.9 (±1.5) MPa for pure HA coating to 26.8 (±2.3) MPa for the HA-TiO₂ composite coating.

The bond strength was found to decrease further to 17.2 (±1.2) MPa as the TiO₂ addition was increased to 20 vol pct. Furthermore, the bond strength of the investigated HA-TiO₂ coating is found to be higher than that reported by Li *et al.*^[12] This result further shows that the investigated flame-spraying technique can give better results compared with the reported HVOF spraying technique.

E. Corrosion Behavior

The potentiodynamic curves of uncoated, HA-coated and HA-TiO₂-coated Ti-6-4 in Ringer's solution at 310 K ± 1 K (37 °C ± 1 °C) temperature are shown in Figure 10. These curves are selected because their data is nearest to the mean values of current densities of the corresponding group of specimens. The corrosion parameters determined from these curves by tafel extrapolation method are summarized in Table III.

The various corrosion parameters are anodic tafel slope (β_a), cathodic tafel slope (β_c), corrosion potential (E_{Corr}), corrosion current density (I_{Corr}), and corrosion rate (C_R). According to Table III, the uncoated Ti-6-4 possesses a higher corrosion current density ($I_{\text{Corr}} = 906 \text{ nAcm}^{-2}$) and, thus, lower corrosion resistance than HA- and HA-TiO₂-coated Ti-6-4. The

Table II. Bond Strength of Thermal-Sprayed HA Coating Techniques

Coating Techniques	Feedstock	Coating Thickness (μm)	Substrate	ASTM Standard	Bond Strength (MPa)	Reference
Plasma spray	HA	120	SS 316 LVM	ASTM C633	60	31
		350	SS 316 LVM	ASTM C633	40	
Plasma spray	HA	180 ± 20	Ti-6-4	ASTM C633	9.18 ± 0.72	32
Plasma spray	HA	150	Ti-6-4	ASTM C633	24.5 ± 2.4	33
HVOF spray	HA	180 ± 15	Ti-6-4	ASTM C633-79	28	12
HVOF spray	NHA	na	Ti-6-4	ASTM C633-01	24 ± 8	34

NHA: nanostructured HA; na: not available.

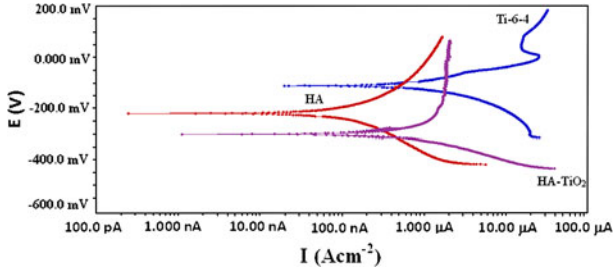


Fig. 10—Potentiodynamic curves of uncoated, flame-sprayed HA, and HA-TiO₂-coated Ti-6-4 in Ringer's solution at 310 K \pm 1 K (37 °C \pm 1 °C).

Table III. Corrosion Parameters Determined by Tafel Extrapolation Method

Parameters	Uncoated	HA Coated	HA-TiO ₂ Coated
β_a (e^{-3} V/decade)	90.80	151.9	48.60
β_c (e^{-3} V/decade)	65.00	109.5	27.90
E_{Corr} (mV)	-112.0	-220.0	-302.0
I_{Corr} (nAcm^{-2})	906.0	120.0	150.0
C_R (mm/year)	0.0157	0.0041	0.0047

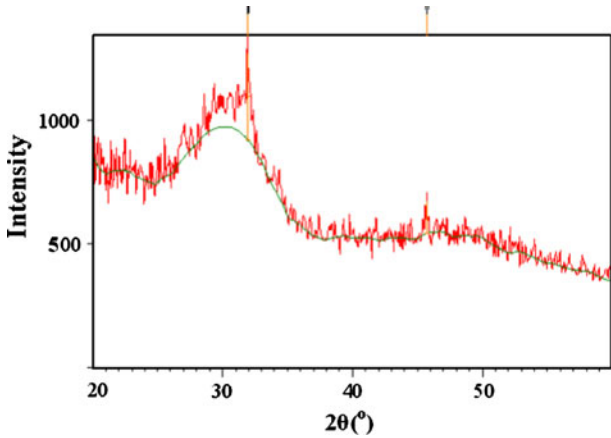


Fig. 11—X-ray diffraction pattern of flame-sprayed HA coating on Ti-6-4, after corrosion testing in Ringer's solution.

polarization curve, for the HA coating (Figure 10), was shifted to the left when compared with uncoated and HA-TiO₂-coated Ti-6-4 curves. It shows that

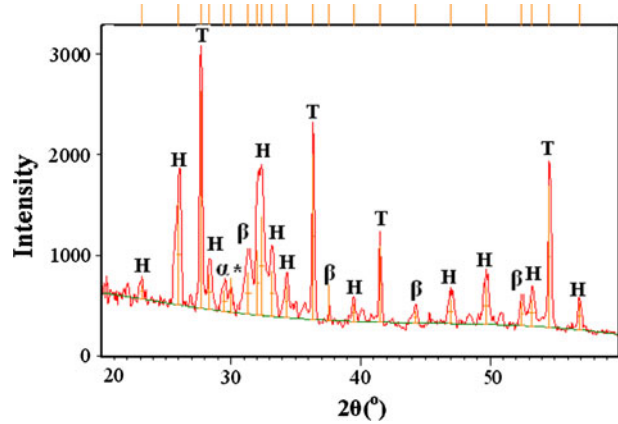


Fig. 12—X-ray diffraction pattern of flame-sprayed HA-TiO₂ coating on Ti-6-4, after corrosion testing in Ringer's solution [HA (H), TiO₂ rutile (T), TTCP (*), α -TCP (α), and β -TCP (β)].

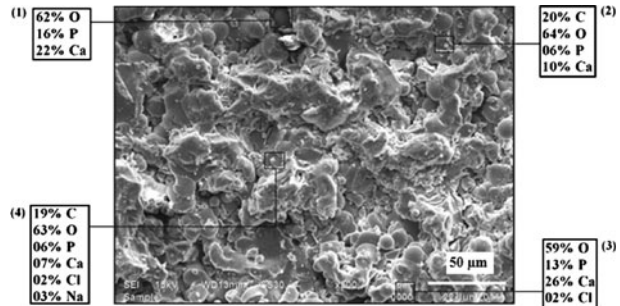


Fig. 13—FE-SEM along with EDS point analysis of flame-sprayed HA-coated Ti-6-4, after corrosion testing in Ringer's solution.

HA-coated specimens are more corrosion-resistant compared with both uncoated and HA-TiO₂-coated Ti-6-4 specimens. The HA-TiO₂ coating decreased the corrosion current density of Ti-6-4 ($I_{\text{Corr}} = 150 \text{ nAcm}^{-2}$) and the corrosion current density of the HA-coated Ti-6-4 decreased further ($I_{\text{Corr}} = 120 \text{ nAcm}^{-2}$). When I_{Corr} is low, passivation is more easily obtained and corrosion resistance is excellent.^[35] Even though all I_{Corr} values reflect excellent corrosion resistance including an uncoated Ti-6-4 specimen, it can be deduced through this study that both HA and HA-TiO₂ coatings have shown improvement in corrosion resistance compared with uncoated Ti-6-4. In another study,^[36] it has been observed that an electrolytic HA/ZrO₂ coating showed

higher corrosion resistance than the HA-coated Ti-6-4 implant material. Similarly, sol-gel-fabricated HA coatings showed improvement in the corrosion resistance of

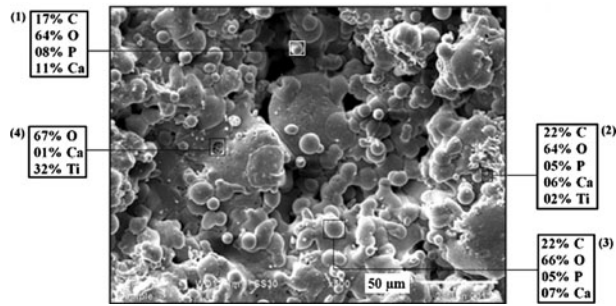


Fig. 14—FE-SEM along with EDS point analysis of flame-sprayed HA-TiO₂-coated Ti-6-4, after corrosion testing in Ringer's solution.

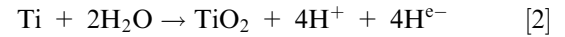
Table IV. Ca/P Ratio of Flame-Sprayed HA and HA-TiO₂ Coatings Before and After Corrosion Testing on Ti-6-4 Substrate

Coating	Point 1	Point 2	Point 3
(a) HA coating (before corrosion testing)	1.64	11.2	1.83
(b) HA coating (after corrosion testing)	1.37	1.67	2.00
(c) HA-TiO ₂ coating (before corrosion testing)	1.50	1.80	1.52
(d) HA-TiO ₂ coating (after corrosion testing)	1.37	1.20	1.40

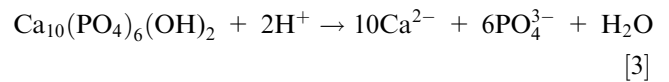
titanium porous scaffolds.^[37] Fathi *et al.*^[38] reported that plasma-sprayed, HA-coated commercially pure titanium (cp Ti) and 316L SS showed a significant effect on corrosion resistance compared with uncoated cp Ti and 316L SS substrates.

Corrosion in HA coatings is associated with the incursion of chloride ion and water into the coating and then subsequent electrochemical reactions at the interface of HA and Ti-6-4.^[39] Each micropore acts as a active site for entrapping surrounding corrosive impurities. Zhang *et al.*^[40] reported the corrosion mechanism of HA coatings with pores and cracks in two steps:

Hydrogen ions (H⁺) are produced at the interface area where corrosion occurs as evident from the following equation



It is then followed by the dissolution of HA in the high concentration area:



After electrochemical corrosion testing in Ringer's solution, the XRD scans of HA-coated (Figure 11) and HA-TiO₂-coated Ti-6-4 (Figure 12) showed an interesting behavior. The HA coating remained amorphous, but some XRD peaks appeared after immersion in Ringer's solution. The HA-TiO₂ coating appeared more crystalline, and it was found that the intensity of the XRD peaks increased after corrosion testing in Ringer's solution. Previously, it was reported that in

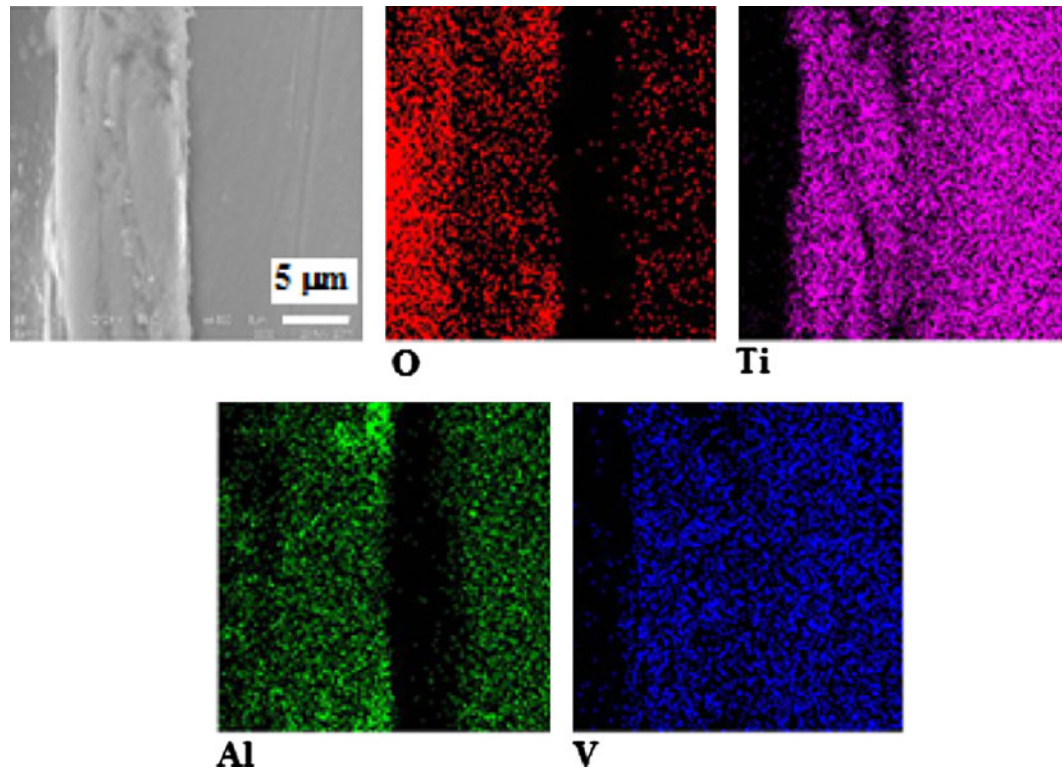


Fig. 15—Cross-sectional EDS elemental maps of uncoated Ti-6-4, after corrosion testing in Ringer's solution.

electrophoretic deposited HA coatings on Ti-6-4 specimens, immersed in Hank's solution at 310 K (37 °C) for 4 weeks, the XRD analysis showed a significant increase in intensity of apatite peaks. The apatite formation reveals the bone bioactive behavior of HA coatings.^[39]

The exposed specimens were examined by SEM/EDS for the microstructural analysis of their scales. Few studies report the microstructure of thermal-sprayed HA coatings after their corrosion testing in Ringer's solution. The microstructure of the corroded HA coating (Figure 13) consists of well-flattened splats with the presence of some spherical-shaped particles. The splats seem to be fused to give a well-bounded appearance. A comparison of the SEM micrographs of the as-sprayed and exposed HA-TiO₂ coating (Figures 6 and 14) showed that the coating has retained its morphology even after exposure to the corrosion testing. An EDS point analysis confirms the presence of Ca, P, O, and C elements in both HA- and HA-TiO₂-coated Ti-6-4 specimens. Except these basic elements, the HA-coated specimen also shows the presence of sodium (Na) and chlorine (Cl). The presence of Na and Cl in EDS spectra (Figure 13) can be attributed to the Ringer's solution as

the specimens were immersed in the solution for their corrosion testing. No cracks are found on the surface of both HA and HA-TiO₂-coated specimens, but some pores are clearly visible on the surface of HA-TiO₂-coated Ti-6-4 specimens after immersion in Ringer's solution. The presence of Ti was also confirmed along with other basic elements in HA-TiO₂-coated specimens (Figure 14). It was also found that after immersion in Ringer's solution, the percentage of O increased in both HA and HA-TiO₂ coatings, which indicates the onset of oxidation. The comparison of both HA and HA-TiO₂ coatings, shows that the quantity of Ca and P decreased after their immersion in Ringer's solution. The Ca/P ratios (in atomic pct) of flame-sprayed HA and HA-TiO₂ coatings before and after corrosion testing are tabulated in Table IV.

The results show the decrease of the Ca/P ratio after immersion in Ringer's solution. The observed different Ca/P ratios confirm the presence of different calcium phosphate compounds. The Ca/P ratio of 1.37 in both the HA (at point 1 in Figure 13) and HA-TiO₂ coatings (at point 1 in Figure 14) is very close to the Ca/P ratio of 1.33, which confirms the formation of octocalcium

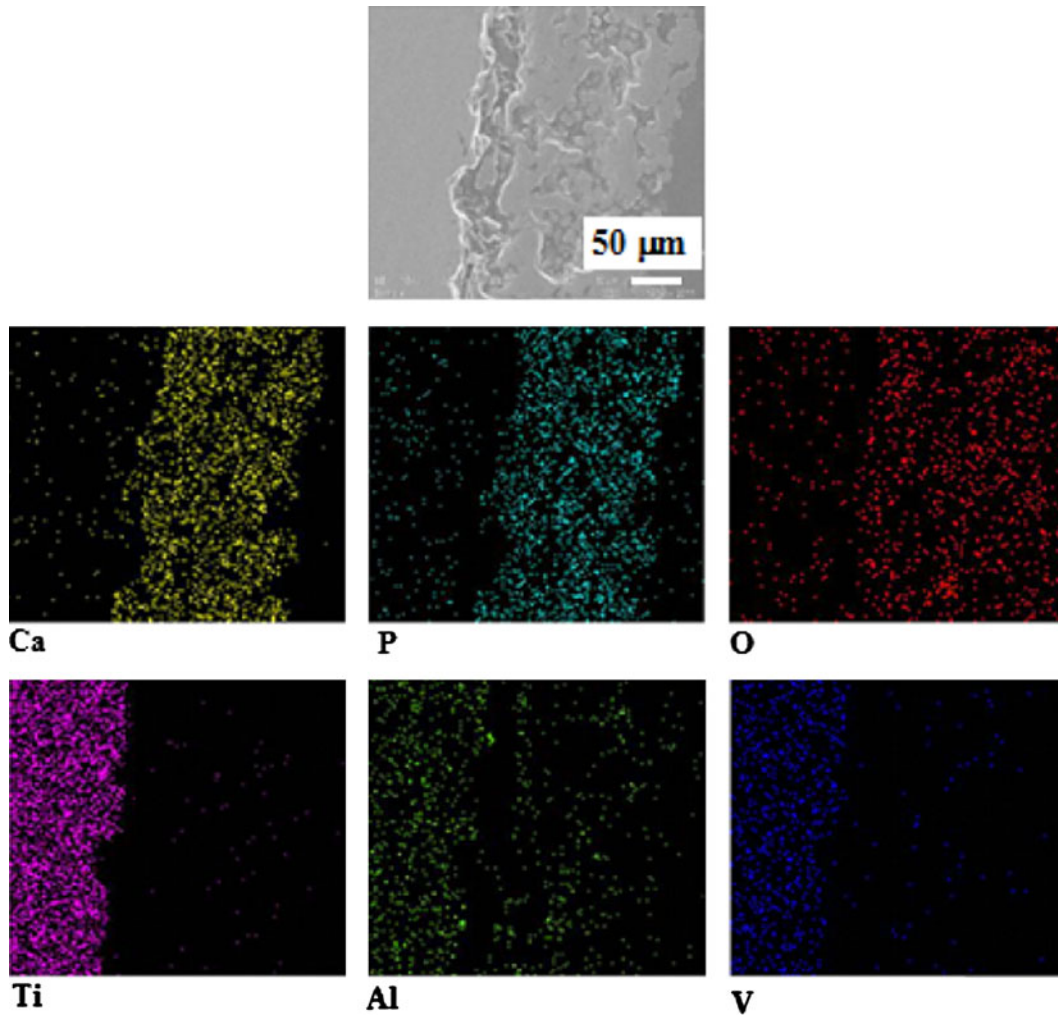


Fig. 16—Cross-sectional EDS elemental maps of flame-sprayed, HA-coated Ti-6-4, after corrosion testing in Ringer's solution.

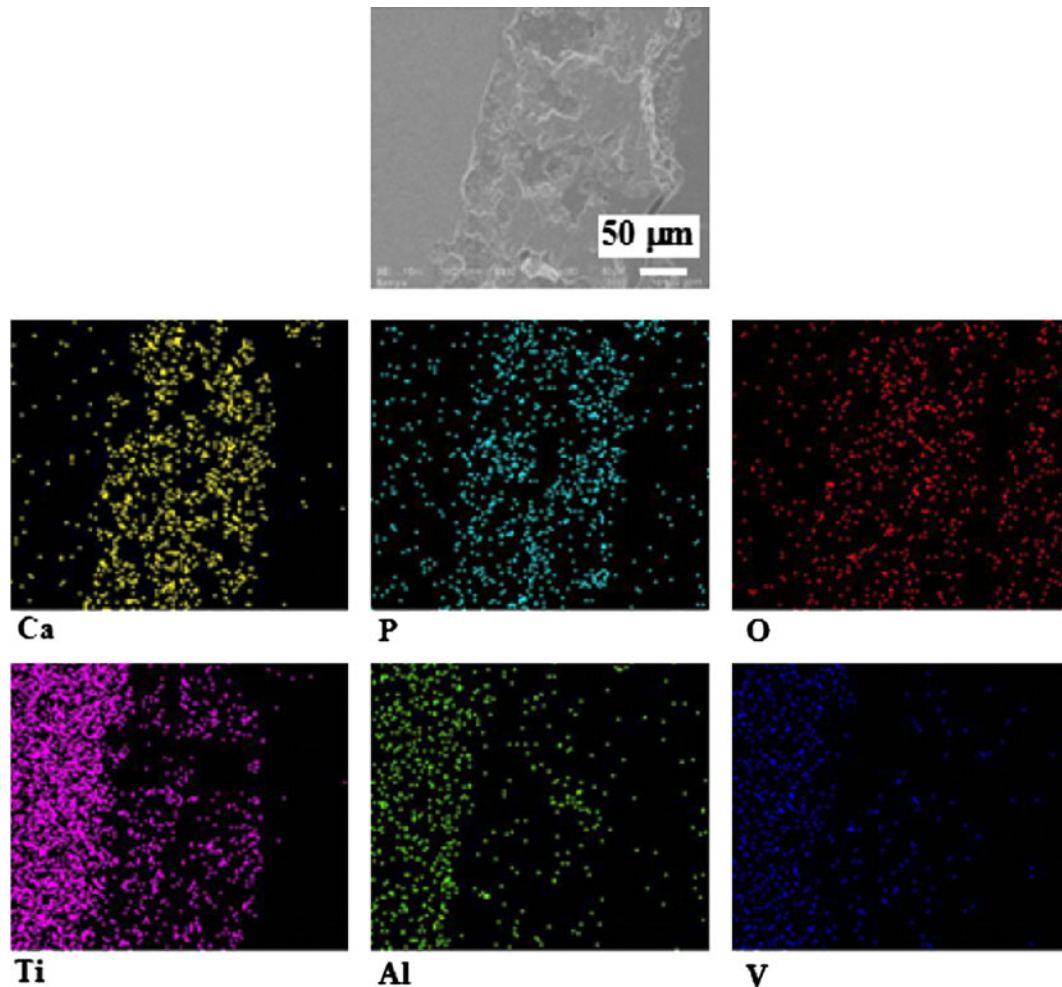


Fig. 17—Cross-sectional EDS elemental maps of flame-sprayed, HA-TiO₂-coated Ti-6-4, after corrosion testing in Ringer's solution.

phosphate. The Ca/P ratio of 2.00 and 1.67 indicates the presence of TCP and HA, respectively.

The cross-sectional microscopic view of uncoated Ti-6-4 substrate (Figure 15) reveals the presence of a dense and uniform oxide scale over the Ti-6-4 substrate after corrosion testing in Ringer's solution. The corrosion behavior of an implant material during its exposure to the human body environment highly depends on the stability of the protective oxide layer. EDS maps confirm the presence of Ti, Al, and V elements in the oxide scale, along with a significant presence of O in outer layers of the scale. This indicates the formation of oxides of Ti, Al, and V. There is an inner band in the scale, which is completely depleted of Al. This result indicates that Al may have preferentially oxidized to form an Al-rich oxide scale at the top of the alloy, leaving an Al-depleted inner band. Some Ti is present, as well as V-depleted zones in the oxide scale; however, the extent is marginal compared with Al. It is pertinent to mention that such depletions are not favorable for any alloy as they may degrade the material properties. The cross section of HA coating (Figure 16) shows a lamellar structure. The coating-substrate interface seems to be defect free. EDS maps show that Ti, Al, and V elements are present in the substrate only without

showing any diffusion into the coating area, which is a desirable characteristic. The presence of Ti is apparent in both the coating and substrate in HA-TiO₂ coating (Figure 17). The O is present throughout in both the coatings. The presence of a few Al-rich spot elements in both the coatings may be caused by Al₂O₃ polishing of coated samples during the sample preparation. The comparison of EDS maps of the as-sprayed (Figures 7 and 8) and exposed (Figures 16 and 17) specimens of both HA and HA-TiO₂ coatings has not shown any significant differences. These observations endorse that both the coatings were successful to retain their adherence and identity even after the corrosion testing. Moreover, the coatings by and large were successful to avert depletion of various base alloy elements during corrosion testing. These observations show that these coatings can be useful to protect the base alloy.

IV. CONCLUSIONS

HA-TiO₂ composite coatings (50:50 wt pct) were developed by thermal-spray technique on Ti alloy substrate. The following conclusions have been drawn from the study:

- In HA-TiO₂ composite coatings, the coating structure is mainly composed of HA and TiO₂ (rutile) phases. Besides the crystalline HA and TiO₂ phases, as-sprayed coating consists of minor β-TCP phase, but no chemical compounds such as CaTiO₃ were detected from the XRD scans. The addition of TiO₂ effectively improved the crystallinity of HA in HA-TiO₂ coating; otherwise, the HA coating was amorphous.
- The SEM/EDS analysis confirmed that both powders HA and TiO₂ melted enough to form a dense and homogeneously distributed HA-TiO₂ composite coating without any crack formation.
- The average value of the HA coating thickness is 120 μm, whereas in HA-TiO₂ coatings, the observed coating thickness is 140 μm. The HA-TiO₂ coatings exhibit a higher roughness (Ra = 8.04 μm) than HA-coated Ti-6-4 (Ra = 3.87 μm). The increase in roughness can be attributed to TiO₂ in composite coating.
- The flame-sprayed HA coating exhibited higher bond strength (67.8 MPa) compared with the investigated HA-TiO₂ coating (37.6 MPa) and other thermal-spray HA-coating techniques reported in literature.
- The electrochemical study showed an improvement in the corrosion resistance of the Ti-alloy after the deposition of flame-sprayed HA and HA-TiO₂ coatings in simulated human body fluid conditions. After corrosion testing in Ringer's solution, the intensity of XRD peaks increased and HA-TiO₂ coating appeared more crystalline.
- The cell culture studies of these coatings are in progress, which would provide useful information regarding their *in vitro* biological behavior and possible applications in the biomedical field.

ACKNOWLEDGMENTS

The work presented in this article has been supported by ISIRD Research Grant from Indian Institute of Technology Ropar, Rupnagar, India. The authors express their gratitude to Metalizing Equipment Company Private Limited (MECPL), Jodhpur, India for providing a flame-spraying (CERAJET) facility to deposit the coatings.

REFERENCES

1. S. Yilmaz, M. Ipek, G.F. Celebi, and C. Bindal: *Vacuum*, 2005, vol. 77 (3), pp. 315–21.
2. M. Niinomi: *Sci. Techno. Adv. Mater.*, 2003, vol. 4 (5), pp. 445–54.
3. M. Songür, H. Celikkan, F. Gökmeşe, S.A. Simşek, N.S. Altun, and M.L. Aksu: *J. Appl. Electrochem.*, 2009, vol. 39 (3), pp. 1259–65.
4. M. Gaona, R.S. Lima, and B.R. Marple: *Mater. Sci. Eng.*, 2007, vol. 458 (1–2), pp. 141–49.
5. G. Manivasagam, D. Dhinasekaran, and A. Rajamanickam: *Recent. Pat. Corr. Sci.*, 2010, vol. 2, pp. 40–54.
6. M.H. Fathi: *J. Mater. Process. Technol.*, 2009, vol. 209 (3), pp. 1385–91.
7. X. Liu, P.K. Chu, and C. Ding: *Mater. Sci. Eng.*, 2004, vol. 47, pp. 49–121.
8. U. Vijayalakshmi, A. Balamurugan, and S. Rajeshwari: *Trends Biomat. Artif. Organs*, 2005, vol. 18 (2), pp. 101–05.
9. L. Le Guehennec, A. Soueidan, P. Layrolle, and Y. Amouriq: *Dent. Mater.*, 2007, vol. 23 (7), pp. 844–54.
10. J.L. Ong, M. Appleford, S. Oh, Y. Yang, W.H. Chen, J.D. Bumhardner, and W.O. Haggard: *J. Miner., Met. Mater. Soc.*, 2006, vol. 58 (7), pp. 67–69.
11. R.R. Kumar and M. Wang: *Mater. Lett.*, 2002, vol. 55 (3), pp. 133–37.
12. H. Li, K.A. Khor, and P. Cheang: *Biomaterials*, 2002, vol. 23 (1), pp. 85–91.
13. H. Li, K.A. Khor, and P. Cheang: *Biomaterials*, 2003, vol. 24 (6), pp. 949–57.
14. X. Nie, A. Leyland, and A. Matthews: *Surf. Coat. Technol.*, 2000, vol. 125 (1–3), pp. 407–14.
15. F.X. Ye, A. Ohmori, T. Tsumura, K. Nakata, and C.J. Li: *J. Therm. Spray Technol.*, 2007, vol. 16 (5–6), pp. 776–82.
16. J. Breme and V. Biehl: *Handbook of Biomaterial Properties: Part II*, J. Black and G. Hastings, eds., Chapman & Hall, London, U.K., 1998, pp. 135–213.
17. A. Ferrer, I. García, J. Fernández, and J.M. Guilemany: *Mater. Sci. Forum*, 2010, vols. 636–637, pp. 82–88.
18. P.A. Ramires, A. Romito, F. Cosentino, and E. Milella: *Biomaterials*, 2001, vol. 22 (12), pp. 1467–74.
19. E. Milella, F. Cosentino, A. Licciulli, and C. Massaro: *Biomaterials*, 2001, vol. 22 (11), pp. 1425–31.
20. K.A. Khor, H. Li, and P. Cheang: *Biomaterials*, 2003, vol. 24 (13), pp. 2233–43.
21. T.A. Vu and R.B. Heimann: *J. Mater. Sci. Lett.*, 1997, vol. 16 (20), pp. 1680–82.
22. L.D. Piveteau, B. Gasser, and L. Schlapbach: *Biomaterials*, 2000, vol. 21 (21), pp. 2193–2201.
23. P. Li, K. Groot, and T. Kokubo: *J. Sol-Gel Sci. Technol.*, 1996, vol. 7, pp. 27–34.
24. H. Li, K.A. Khor, and P. Cheang: *Surf. Coat. Technol.*, 2002, vol. 155, pp. 21–32.
25. H.W. Kim, H.E. Kim, V. Salih, and J.C. Knowles: *J. Biomed. Mater. Res. B, Appl. Biomater.*, 2005, vol. 72 (1), pp. 1–8.
26. F.J. Gil, A. Padros, J.M. Manero, C. Aparicio, M. Nilsson, and J.A. Planell: *Mater. Sci. Eng.*, 2002, vol. C22, pp. 53–60.
27. K.A. Gross, C.C. Berndt, D.D. Goldschlag, and V.J. Iacono: *Int. J. Oral Maxillofac. Implants*, 1997, vol. 12 (5), pp. 589–97.
28. J. Weng, X. Liu, X. Zhang, and X. Ji: *J. Mater. Sci. Lett.*, 1994, vol. 13 (3), pp. 159–61.
29. M. Miyayama, K. Koumoto, and H. Yanagida: *Engineered Materials Handbook, Ceramic and Glasses*, vol. 4, S.J. Schneider, ed., ASM International, Materials Park, OH, 1991, pp. 748–57.
30. Z. Mohammadi, A.A. Ziaei-Moayyed, and A. Sheikh-Mehdi Mesgar: *Mater. Proc. Technol.*, 2007, vol. 194, pp. 15–23.
31. M. Vilotjević, P. Marković, S. Zec, J.S. Marinkovic, and V. Jakanovic: *Mater. Process. Technol.*, 2011, vol. 211 (6), pp. 996–1004.
32. Y.C. Yang and E. Chang: *Biomaterials*, 2001, vol. 22 (13), pp. 1827–36.
33. S.W.K. Kweh, K.A. Khor, and P. Cheang: *Biomaterials*, 2002, vol. 23 (3), pp. 775–85.
34. R.S. Lima, K.A. Khor, H. Li, P. Cheang, and B.R. Marple: *Mater. Sci. Eng.*, 2005, vol. 396 (1–2), pp. 181–87.
35. A.M. Al-Mayouf, A.A. Al-Swayih, N.A. Al-Mobarak, and A.S. Al-Jabab: *Mater. Chem. Phys.*, 2002, vol. 14 (2–3), pp. 118–25.
36. S.K. Yen, S.H. Chiou, S.J. Wu, C.C. Chang, S.P. Lin, and C.M. Lin: *Mater. Sci. Eng.*, 2006, vol. 26 (1), pp. 65–77.
37. S.C.P. Cachinho and R.N. Correia: *J. Mater. Sci. Mater. Med.*, 2008, vol. 19 (1), pp. 451–57.
38. M.H. Fathi, M. Salehi, A. Saatchi, V. Mortazavi, and S.B. Moosavi: *Dent. Mater.*, 2003, vol. 19 (3), pp. 188–98.
39. C.T. Kwok, P.K. Wong, F.T. Cheng, and H.C. Man: *Appl. Surf. Sci.*, 2009, vol. 255 (13–14), pp. 6736–44.
40. Z. Zhang, M.F. Dunn, T.D. Xiao, A.P. Tomsia, and E. Saiz: *Nanotech. Biotech. Convergence*, Stamford, CT, 2002, pp. 291–96.